# In Situ Electrochemical Investigation of Pyrite Assisted Leaching of Chalcopyrite

**Qingyou Liu,[1] Miao Chen,[2] Kai Zheng,[1,3] Yi Yang,[2] Xiaonan Feng,[1,3] and Heping Li [1,z]**

[1] *Key Laboratory of High-temperature and High-pressure Study of the Earth's Interior, Institute of Geochemistry, Chinese Academy of Sciences, Guiyang 550081, People's Republic of China*
[2] *CSIRO Mineral Resources Flagship, Clayton, Victoria 3169, Australia*
[3] *University of Chinese Academy of Sciences, Beijing 100049, People's Republic of China*

Chalcopyrite is not only the most abundant but also one of the most refractory sources of copper. In this study, leaching experiments showed that leaching efficiency increases with increasing amounts of pyrite. In the absence of the addition of pyrite, chalcopyrite was leached at an approximate rate of 0.03 g/L/day. This rate increased to approximately 0.29 g/L/day when the pyrite/chalcopyrite (Py/Cp) weight ratio was 5. Polarization curves show that the $i_{couple}/i_{corr}$ value was 1.71 at a cathode to anode ($S_c/S_a$) area ratio of 1:1. Galvanic corrosion tests of current confirmed that the chalcopyrite leaching selectivity improved with an increasing Py/Cp ratio. Electrochemical impedance spectroscopy (EIS) results showed that the chalcopyrite electrochemical dissolution (leaching) rate depended on the charge transfer at the double layer and the passive film characteristics and that the chalcopyrite corrosion rate decreased as soak time increased. The presence of pyrite promotes the electrochemical dissolution of chalcopyrite and results in galvanic protection.

 [DOI: 10.1149/2.0461813jes]

Manuscript submitted July 17, 2018; revised manuscript received August 29, 2018. Published September 21, 2018.

Galvanic corrosion is an electrochemical process; indeed, when two metals are put in contact with each other in a conducting medium, one metal preferentially undergoes corrosion, while the other metal is protected. The difference in the rest potentials between the two metals determines the selectivity during corrosion. The less noble metal, which has a lower rest potential, undergoes corrosion. Galvanic interaction is used in mineral processing to improve the flotation efficiency[1,2] and hydrometallurgy recovery of valuable metals.[3] The latter is the focus of this paper.

Chalcopyrite is not only the most abundant but also one of the most refractory copper sources. To date, the leaching kinetics of chalcopyrite are slow and remain to be a challenge.[4] Galvanic interaction has been shown to be an effective means to enhance the efficiency of copper extraction from chalcopyrite. To exploit galvanic interaction in chalcopyrite leaching, chalcopyrite is intentionally mixed with a second mineral with a higher rest potential, such as pyrite. Acceleration by a factor of 2 to 15 in chalcopyrite leaching was reported when pyrite was added to a leaching medium.[5,6] The Galvanox process is a commercial technology based on galvanic interaction whereby 98% chalcopyrite recovery can be achieved in as little as four hours at atmospheric pressure with a temperature of 70°C.[7] Olvera et al.[8] investigated the effect of pyrite on the electrochemical dissolution of fresh and passivated chalcopyrite. They pointed out that $FeS_2$ increased the dissolution rate of fresh and passivated $CuFeS_2$ electrodes, indicating that the galvanic effect continued even after the electrode was chemically passivated. The dissolution rate of the fresh $CuFeS_2$ electrode was controlled by the reduction of $Fe^{3+}$ ions, whereas for the passivated $CuFeS_2$ electrode, the dissolution rate was controlled by diffusion within the passive film. Li et al.[9] considered chalcopyrite dissolution according to the examination of the evolution of sulfur species, with and without pyrite, depending on scanning photoelectron microscopy. The results revealed that when chalcopyrite contacted pyrite, significantly greater chalcopyrite surface oxidation than that for the other systems examined was observed, with $S^0$, $SO_3^{2-}$ and $SO_4^{2-}$ being identified as heterogeneous across the surface. It has been proposed that chalcopyrite oxidative dissolution is enhanced by increasing its cathodic area. The high degree of surface heterogeneity of these surface products indicates that these surfaces are not passivated by their formation.

As mentioned above, the process of pyrite-assisted chalcopyrite leaching is well documented, but the in situ electrochemical characteristics of chalcopyrite and pyrite during a galvanic reaction requires further study. In this paper, three experiments were processed: (1) pyrite-assisted leaching of chalcopyrite experiment, with an aim to investigate the quantitative effect of the pyrite-assisted leaching of chalcopyrite, (2) electrochemical experiment, that is, depending on in-situ potentiodynamic polarization, EIS and galvanic current measurements, to reveal the mechanism of chalcopyrite electrochemical dissolution and the interaction involved in the galvanic effect, and how and to what extent $S_c/S_a$ (area ratio of cathode to anode) affect pyrite-chalcopyrite galvanic interaction, and (3) Raman spectroscopy measurements, with a purpose to analyze the corrosion products.

## Experimental

***Mineral preparation.***—Chalcopyrite and pyrite were obtained from Mt Lyll, Australia and North Dakota, USA, respectively. The concentrates had less than 4% impurities, as confirmed by Powder X ray diffraction (XRD) and chemical analysis.[10] Powder samples for the leaching experiment were grounded to −200 meshes before use. Pyrite and chalcopyrite electrodes were prepared by cutting the pyrite and chalcopyrite samples into cubes; the working area of chalcopyrite was 0.2 $cm^2$, and the working areas of pyrite were 0.8, 0.4, 0.2 and 0.1 $cm^2$. As far as possible, the chosen specimens did not display imperfections. They were placed into epoxy resins and were connected to a copper wire by silver paint on the back face, leaving one top face of the electrode exposed to the solution. Before each test, the exposed face of the electrode was polished, and a fresh surface was used. MilliQ-treated water was used for sample preparation.

***Leaching experiments.***—Galvanic leaching tests were carried out in 250 mL Erlenmeyer flasks. One hundred and fifty milliliters of modified 9K media containing 0.75 g/L $FeSO_4 \cdot xH_2O$, 2.25 g/L $Fe_2(SO_4)_3 \cdot xH_2O$, 3.0 g/L $(NH_4)_2SO_4$, 0.5 g/L $MgSO_4 \cdot 7H_2O$, 0.5 g/L $K_2HPO_4$, 0.1 g/L KCl and 0.01 g/L $Ca(NO_3)_2$ was prepared. Six leaching tests were carried out (Table I). The amount of chalcopyrite used, when required, was 1.2 g. The pH value of these solutions was 1.8, which was adjusted with sulfuric acid (98%, wt%). Every three to five days, water was added due to evaporation. The solution pH and redox potential were monitored using a Mettler Toledo Multi Seven unit. Approximately 2 ml of leaching solution was removed for $Cu^{2+}$, $Fe^{2+}$, and $Fe_{tot}$ (total iron) ion concentration analysis. The $Cu^{2+}$ concentration was determined using Inductively Coupled Plasma Optical Emission Spectrometry (ICP-OES),[10] and the ferrous and total iron concentrations were determined using the O phenonthroline method spectroscopically (ALS SEC2000 spectrophotometer).[11]

[z] E-mail: liheping@vip.gyig.ac.cn

**Table I. Sample prepared for the leaching experiment.**

| Sample* | Chalcopyrite (g) | Pyrite (g) | Py/Cp (w/w) |
|---|---|---|---|
| 1 | 1.2 | 0 | 0 |
| 2 | 1.2 | 0.6 | 0.5 |
| 3 | 1.2 | 1.2 | 1 |
| 4 | 1.2 | 3.6 | 3 |
| 5 | 1.2 | 6 | 5 |
| 6 | 0 | 1.2 | - |

*Volume = 150 ml, $Fe_{tot} = 3\ g \cdot L^{-1}$, $[Fe^{2+}]/[Fe^{3+}] = 3$.

Powder XRD data were collected in Bragg-Brentano geometry on finely ground samples using a Phillips X'Pert diffractometer fitted with a Co long-fine-focus tube operated at 40 kV and 40 mA and a curved graphite postdiffraction monochromator. The data were collected over the range $5 < 2\theta < 140°$ in steps of $0.02° 2\theta$. The relative proportions of the crystalline phases in each sample were determined using the Rietveld-based quantitative phase analysis (QPA) using Total Pattern Analysis Solution (TOPAS) Version 4.2.[12]

***Electrochemical measurements.***—Electrochemical measurements were performed using a computer-controlled electrochemical measurement system (PARSTAT 2273, Princeton Applied Research) with a conventional three-electrode electrolytic cell that included a platinum auxiliary electrode, a pyrite/chalcopyrite working electrode and a saturated calomel reference electrode (SCE). To minimize the resistance of solution between the working electrode and the reference electrode, the reference electrode was connected to a Luggin capillary. All data of the testing potentials corresponded to SCE.

Polarization curves and EIS tests were used to investigate the electrochemical characteristics of galena weathering. The polarization curves were obtained by automatically changing the electrode potential from −250 to +1000 mV (vs. open current potential, OCP) at a scan rate of $5\ mV \cdot s^{-1}$. The EIS tests were performed using the OCP in the frequency range of 100 KHz to 10 mHz with a peak-to-peak amplitude of 5 mV. Then, ZSimpWin 3.20 software was used to fit the impedance data.

During galvanic corrosion current measurements, an electric wire educed from PAR 2273 connected the reference electrode with the auxiliary electrode and then connected the pyrite electrode, while the chalcopyrite was connected to the working electrode. A Luggin capillary connected to SCE was used to keep a distance of 1–2 mm to the working electrode. A schematic circuit diagram for the measurement of galvanic corrosion current is shown in Figure 1.

The electrolyte was a modified 9K media, as state above, and all the chemicals were analytical grade reagents. Each measurement was carried out twice to check the repeatability of the experiments. The experiments were conducted at 25 ± 1°C.

***Raman spectroscopy measurements.***—The surface morphologies of the corroded samples were investigated by Raman spectroscopy. Two pieces of pyrite and two pieces of chalcopyrite (the sizes were all

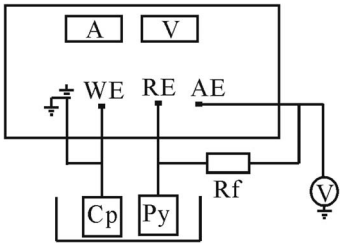


**Figure 1.** Schematic circuit diagram for the measurement of galvanic corrosion current.

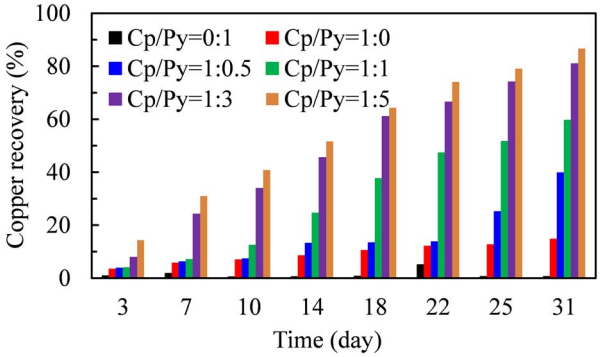


**Figure 2.** Copper ion concentration and copper recovery as a function of time for the galvanic leaching of chalcopyrite.

1.0 cm × 1.0 cm × 0.2 cm) samples were used for surface analysis. The four galena samples were divided into three groups: (1) pyrite sample alone, (2) chalcopyrite sample alone, and (3) pyrite and chalcopyrite samples contacting each other through a surface; the samples were immersed in 3 bottles of 9K solutions. After being weathered for 5 days, the 3 sample groups were characterized using Raman spectroscopy (British Renishaw inVia Reflex type microscopic confocal laser Raman spectrometer) at a wavelength of 514 nm and a collection time of 10 s. The laser power was 50 mW to avoid the destruction of the galena samples.

## Results and Discussion

***Leaching experiments.***—The copper concentration in the leaching solution increased with time due to the dissolution of chalcopyrite (Figure 2). In the absence of the addition of pyrite (Py/Cp, weight ratio of Pyrite/Chalcopyrite, W/W = 0), chalcopyrite was leached at an approximate rate of 0.03 g/L/day. When pyrite was added to the leaching system (Py/Cp = 0.5 to 5), chalcopyrite leaching enhanced as the copper dissolution rate increased. When Py/Cp equalled 0.5 and 1, an induction period of approximately 20 and 10 days, respectively, was required before the benefits of galvanic leaching could be observed, as indicated by the increase in the rate of copper ion concentration in the solution. Their estimated chalcopyrite dissolution rate was 0.23 and 0.26 g/L/day, respectively. The induction period was not present when the Py/Cp ratio was 3 and 5, where the chalcopyrite leaching rate increased to approximately 0.29 g/L/day. An improvement in chalcopyrite leaching kinetics of up to 9 times can be obtained through exploiting galvanic interaction in chalcopyrite leaching. The results corresponded with the leaching results reported by Mehta and Murr,[5,6] they found that the leaching rates reached 2 to 15 times in chalcopyrite leaching when pyrite was added.

Galvanic interaction was exploited in the leaching of chalcopyrite through the addition of pyrite. During the dissolution of chalcopyrite, the electrochemical anodic half-cell reactions involved chalcopyrite oxidation, and the cathodic half-cell reaction involved the reduction in ferric ion.[13]

$$CuFeS_2 \rightarrow Cu^{2+} + Fe^{2+} + 2S^0 + 4e^- \quad [1]$$

$$4Fe^{3+} + 4e^- \rightarrow 4Fe^{2+} \quad [2]$$

In the absence of pyrite, both reactions occurred at the chalcopyrite surface. The cathodic half-cell reaction was the rate-limiting step for chalcopyrite dissolution.[14] With the addition of pyrite, the cathodic half-cell reaction took place on the pyrite surface at a significantly faster rate, and therefore, the chalcopyrite dissolution rate increased.

The leaching efficiency increases with an increasing amount of pyrite or Py/Cp ratio (Figure 2). With the presence of an increasing amount of pyrite, there is a higher chance for chalcopyrite and pyrite

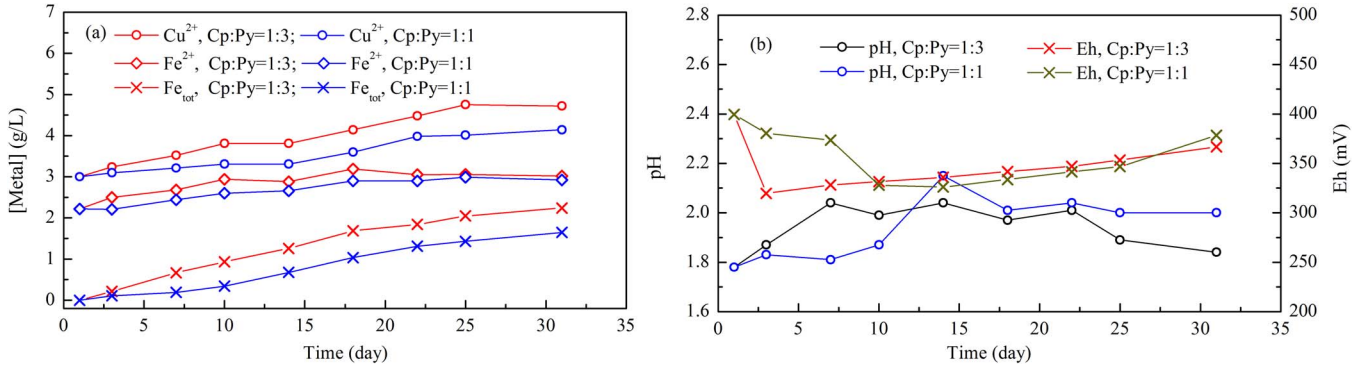


**Figure 3.** The (a) copper, ferrous and total iron ion concentration, and the (b) pH and redox potential of the leaching solution.

to be in electrical contact. Thus, the galvanic interaction is more significant, and the chalcopyrite leaching rate increases accordingly.

The metal ion concentrations, pH and $E_h$, in the leaching solution for two selective leaching experiments (Py/Cp = 1 and 3 at pH 1.8) are shown in Figure 3. With increasing leaching time, the copper, ferrous and total ion concentrations in the leaching solution increase due to mineral (chalcopyrite and/or pyrite) dissolutions. A corresponding increase in solution pH at the initial stage of the leaching is typically found during chalcopyrite dissolution or ferrous oxidation.[15] The decrease in solution $E_h$ at the early stage of leaching is linked to the consumption of $Fe^{3+}$ due to mineral dissolution. This dissolution has also been observed by Córdoba et al.[16] The solution $E_h$ maintained a range of 340–390 mV during the course of leaching, and this range was close to the optimal condition for chalcopyrite leaching.[17]

The QPA of the selective leached residue collected after 31 days of leaching is summarized in Table II. The chalcopyrite leaching selectivity improved with increasing Py/Cp ratio. The ratio of pyrite to chalcopyrite in the leached residue increased from 1.7 to 12 when Py/Cp was increased from 1 to 3. This increase is consistent with the notion that galvanic leaching enhances the leaching of chalcopyrite by depressing the leaching of pyrite.

***Open circuit potential.—***The open circuit potential is often used to evaluate the electrochemical behavior of mineral surfaces. To sulfide mineral electrodes, the OCP consists of a cathodic reduction of dissolved oxygen and an anodic oxidation of the sulfide mineral.[18]

Figure 4 shows the OCP curves of pyrite, chalcopyrite and chalcopyrite coupled with pyrite electrodes in 9K solution as a function of time. The mineral electrodes reached a quasi-steady state (varied less than 2 mV/min) after initiation for approximately 10 min, meaning that there was a spontaneous growth of a passive film on the surface of the electrodes. The OCP of pyrite and chalcopyrite electrodes was approximately 421.32 ± 5 mV and 320.63 ± 5 mV, respectively. A more negative OCP of the chalcopyrite electrode meant that it would act as a cathode when connected with pyrite. When the chalcopyrite electrode was coupled with the pyrite electrode, we saw a similar potential-time profile, and the OCP was 382.4 ± 5 mV between the chalcopyrite and the pyrite electrode, in agreement with the mixed potential theory.[19]

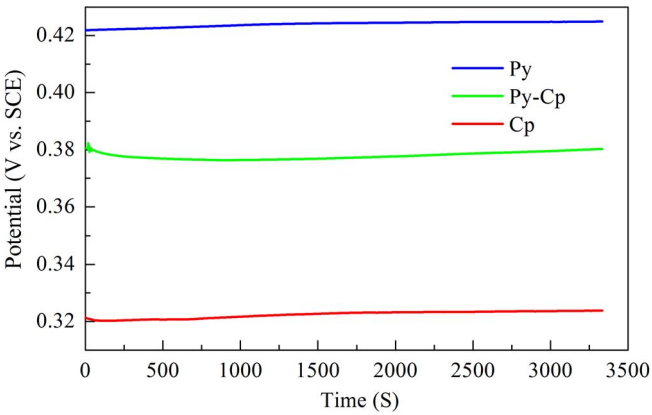


**Figure 4.** Potential-time relationships of the different mineral electrodes in 9K solution.

***Galvanic corrosion.—***Figure 5 shows the potentiodynamic polarization curves obtained for pyrite and chalcopyrite in 9K solution at an area ratio of cathode to anode ($S_c/S_a$) of 1:1. Figure 5 shows that pyrite and chalcopyrite were all easily passivated. Corrosion potential ($E_{corr}$) and corrosion current density ($i_{corr}$) were dependent on the Tafel extrapolation.[20] The experimental values of these parameters are shown in Table III. The results show that the corrosion current densities of pyrite and chalcopyrite were 40.79 and 4.99 $\mu A \cdot cm^{-2}$, respectively, which characterized the two minerals, namely, pyrite, as easily corroded. Furthermore, the corrosion potentials of pyrite and chalcopyrite were 381.36 and 281.91 mV, respectively. The corrosion potentials determined from the polarization curves were significantly lower than those obtained from the open circuit potential measurements, that is, 421.32 ± 5 mV and 320.63 ± 5 mV, respectively. This outcome was due to polarization tests being started at a cathodic potential relative to the corrosion potential so that the passive film at the surface was at least partially removed due to the highly reducing initial potentials. This phenomenon occurs frequently in the corrosion of metal material.[21]

The most important character of the kinetics of the galvanic corrosion-anodic material dissolution rate, according to the Butler-

**Table II. Summary of the QPA of the selectively leached residue collected after 31 days of leaching.**

| Initial leaching condition | | Abiotic leaching residue (%) | | | | | | |
|---|---|---|---|---|---|---|---|---|
| Py/Cp | pH | Pyrite | Chalcopyrite | Quartz | Sulfur | Jarosite | Cu recovery (%) | Py/Cp final |
| 1 | 1.8 | 60.8 | 35.5 | 0.6 | 3.2 | 0 | 62 | 1.7 |
| 3 | 1.8 | 81.4 | 6.8 | 0.7 | 11.1 | 0 | 84 | 12 |

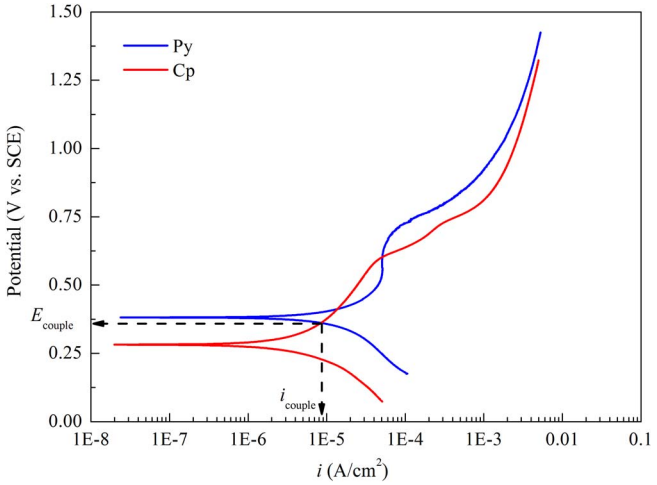


**Figure 5.** Potentiodynamic curves of the pyrite/chalcopyrite electrode in 9K solution.

Volmer equation,[20] can be expressed as Equation 3,[22] which suggests that the anodic material dissolution rate can be estimated by $i_a$, where $i_g$ is the galvanic current density or the coupled current density ($i_{couple}$); $b_a$ and $b_c$ are the Tafel slopes of the anodic reaction and cathodic reaction of chalcopyrite, respectively; $E_{corr}$ is the free corrosion of chalcopyrite; and $E_a$ is the polarization potential of chalcopyrite. Generally, in the metal corrosion field, the ratio $i_{couple}/i_{corr}$ is seen as a guide to reflect the severity of the galvanic effect, and it was suggested that a $i_{couple}/i_{corr}$ value lower than 5 implies compatibility with the members in a galvanic pair.[23] It is worth noting that the coupled potential ($E_{couple}$) or galvanic potential ($E_g$), as well as the coupled current density ($i_{couple}$) or galvanic current density ($i_g$) values of the pair, were estimated from the polarization curves by superimposing the anodic branch of chalcopyrite to the cathodic branch of pyrite. The results show that the $i_{couple}$ and $E_{couple}$ values were 8.53 $\mu A \cdot cm^{-2}$ and 360.71 mV, respectively. The $i_{couple}/i_{corr}$ value was 1.71, suggesting that the chalcopyrite corrosion rate increased to 1.71 times that when coupled with pyrite. Compared with metal corrosion, as semiconductor minerals, the galvanic corrosion of the chalcopyrite/pyrite pair in 9K solutions was not severe.

$$i_g/i_a = 1\text{-}\exp\left[-\frac{2.303(b_a+b_c)(E_a - E_{corr})}{b_a}\right] \quad [3]$$

Figure 6 shows the galvanic corrosion current curves (a) and the corrosion current density $i_g$ (b) for the pyrite-chalcopyrite pair at different area ratios of pyrite to chalcopyrite ($S_c/S_a$). Figure 6a shows similar trends with the curves of the galvanic corrosion current vs. time, a stable state was reached after approximately 6000 S. Furthermore, Figure 6b shows that the $i_g$ and $S_c/S_a$ had a good linear relationship. The $i_g$ was 8.32 $\mu A \cdot cm^{-2}$ at an $S_c/S_a$ of 1/1 (the areas of chalcopyrite and pyrite were all 0.2 cm$^2$), which was close to the result estimated from the polarization curves, namely, $i_{couple}$ being 8.53 $\mu A \cdot cm^{-2}$ and the standard deviation being 2.4%. The detailed galvanic corrosion currents $i_g$ are shown in Table IV. The results corresponded with the above leaching results; namely, the chalcopyrite leaching selectivity improved with an increasing Py/Cp ratio, and explained the above results of Li et al.,[9] who proposed that chalcopyrite oxidative dissolution was enhanced by increasing its cathodic area.

To understand the chalcopyrite electrochemical corrosion processes of diffusion and faradaic reactions at electrodes, EIS studies were used. First, chalcopyrite electrodes (0.2 cm$^2$) and pyrite electrodes (0.2 cm$^2$) were connected through a copper wire, and the two electrodes were soaked in 9K solution for 5 days. Every day, the copper wire connection was broken, and the chalcopyrite electrode and pyrite electrode acted as working electrodes for the EIS tests. A platinum sample acted as an auxiliary electrode, and a SCE acted as a reference electrode.

Figure 7 shows the Bode plot diagram and a typical Nyquist diagram for the chalcopyrite and chalcopyrite/pyrite coupled electrode obtained in a 9K solution after the chalcopyrite coupled with pyrite in galvanic corrosion for 5 days. The Bode plots displayed similar shapes, consisting of 2 time constants. Two quasi-semicircles were reflected in the Nyquist plots, the high frequency region displayed quick responses from the passivation film, and the lower frequency region displayed slow responses from the electric double layer and Faraday processes. The electrochemical equivalent circuit (EEC) shown in Figure 8 was

**Table III. Electrochemical parameters for the mineral electrodes in 9K solutions.**

| Electrode | $E_{corr}$ (mV) | $i_{corr}$ ($\mu A \cdot cm^{-2}$) | $b_c$ (mV) | $b_a$ (mV) | $E_{couple}$ (mV) | $i_{couple}$ ($\mu A \cdot cm^{-2}$) | $i_{couple}/i_{corr}$ |
|---|---|---|---|---|---|---|---|
| Pyrite | 381.36 | 40.79 | 489.97 | 376.92 | 360.71 | 8.53 | 1.71 |
| Chalcopyrite | 281.91 | 4.99 | 141.45 | 268.01 | | | |

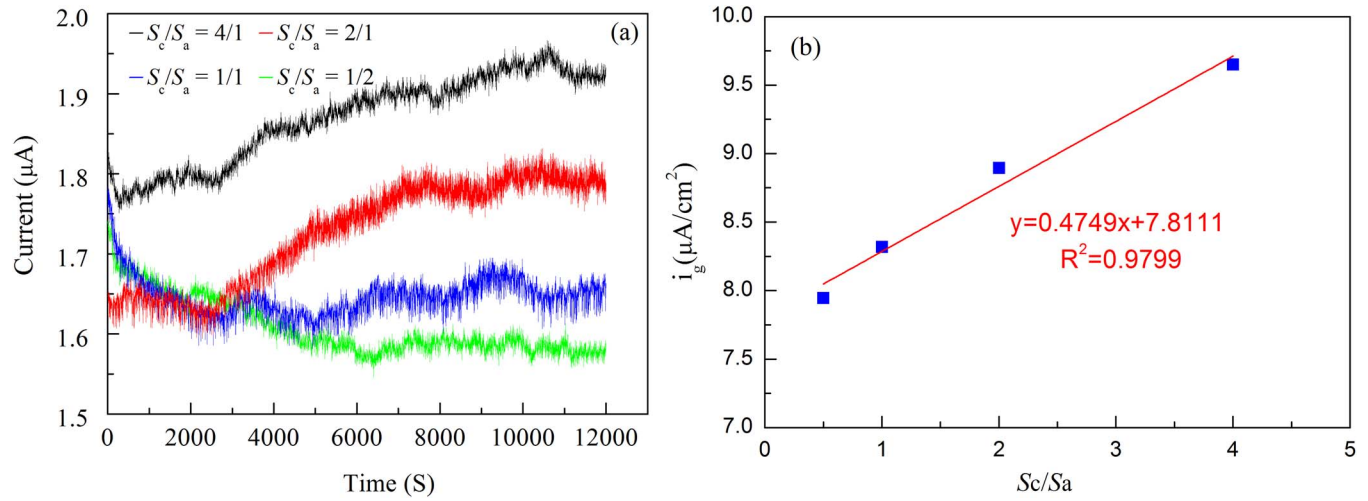


**Figure 6.** The curves of galvanic corrosion current vs. time in the rations of (1) $S_c/S_a$ = 4/1, (2) $S_c/S_a$ = 2/1, (1) $S_c/S_a$ = 1/1, (1) $S_c/S_a$ = 1/2.

**Table IV. Galvanic current in the different area of rations of $S_c/S_a$ under a stable state.**

| $S_c/S_a$ | $i_g$ ($\mu A \cdot cm^{-2}$) |
|---|---|
| 4:1 | 9.65 |
| 2:1 | 8.89 |
| 1:1 | 8.32 |
| 1:2 | 7.95 |

used to model the chalcopyrite/electrolyte interface. In this EEC, $R_s$ was the ohmic resistance of the solution, $R_t$ was the charge transfer resistance, $R_f$ was the passive film resistance, and $CPE_{dl}$ and $CPE_f$ represented the constant phase elements used to replace the charge transfer capacitance at the double layer ($C_{dl}$) and the passive film capacitance ($C_f$), respectively. The impedance of the *CPE* was given by Macdonald as Equation 4,[24] and the conversion relation of *CPE* and *C* was expressed as Equation 5.[25]

$$Z_{CPE} = \frac{1}{Y_0(j\omega)^n} \quad [4]$$

$$C = Y_0^{1/n} \cdot R^{(1/n-1)} \quad [5]$$

Here, $Z_{CPE}$ was the impedance of the constant phase element ($\Omega \cdot cm^2$), $\omega$ was the angular frequency of the AC voltage ($rad \cdot s^{-1}$), $Y_0$ was the magnitude of admittance of the *CPE* ($\Omega^{-1} \cdot cm^{-2} \cdot S^{-n}$), and $n$ was a dimensionless number. When $n = 1$, the capacitance was considered to be ideal. The impedance parameters obtained by fitting the EIS data to the equivalent circuit are listed in Table V. The impedance parameters showed, when soak time increased, that the charge transfer resistance ($R_t$) increased, meaning that the charge transfer changed, which became difficult at the double layer. Additionally, the passivation resistance ($R_f$) increased, and the passive capacitance ($C_f$) decreased. The high resistance and low capacitance of the films on the electrode indicated the relatively better robustness of the passive film. These results revealed that the chalcopyrite corrosion rate decreased when soak time continued. Compared the results of pyrite-chalcopyrite galvanic with the results of chalcopyrite self-corrosion, at an identical soak time, even the passivation film has been occurred, the pyrite-chalcopyrite galvanic always had smaller charge transfer resistance ($R_t$) and larger charge transfer capacitance ($C_t$), meaning that the galvanic effect still existed even chalcopyrite was passivated.[8]

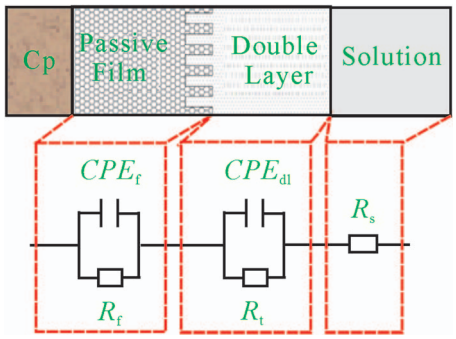


**Figure 8.** Equivalent circuit for the chalcopyrite and chalcopyrite-pyrite electrode in 9K solutions.

Figure 9 shows the Bode plot diagram and a typical Nyquist diagram for galvanic-protected pyrite obtained in 9K solution. The experimental results showed that the Bode curves or the Nyquist curve was almost overlapped completely (only three Bode/Nyquist curves are shown, as the others overlapped completely). The result revealed that pyrite undergoes cathodic protection during the soaking process. Specifically, three time constants were clearly observed from the Bode curves, and three capacitive loops were reflected in the Nyquist curve. Considering that pyrite is characterized by an absorbable character,[26,27] we could deduce that, except for the charge transfer and passive processes, the third time constant should involve ions being adsorbed on the pyrite surface. The equivalent circuit used to model the pyrite/electrolyte interface is shown in Figure 10. $R_s$ was the ohmic resistance of the solution, $R_t$ was the charge transfer resistance, and $CPE_{dl}$ was the double-layer capacitance. $R_{sl}$ and $CPE_{sl}$ referred to the adsorption species, such as the iron-containing compounds. $R_f$ was the pore resistance of the film, and $CPE_f$ corresponded to the capacitance of the passive film. Such a model had previously been used by Velásquez et al.[28] to model the interfacial behavior of pyrite in the alkaline solutions. The EIS experimental results are shown in Table VI. During these electrochemical parameters, the smallest resistance and the largest capacitance were $R_{sl}$ and $C_{sl}$ from the adsorption species, while the largest resistance and the smallest capacitance were $R_t$ and $C_t$ from the double layer. The results revealed that the adsorption process easily occurred, while the charge transfer in the double layer was difficult. That is, pyrite electrochemical dissolution was difficult. Furthermore, the Bode curves and Nyquist

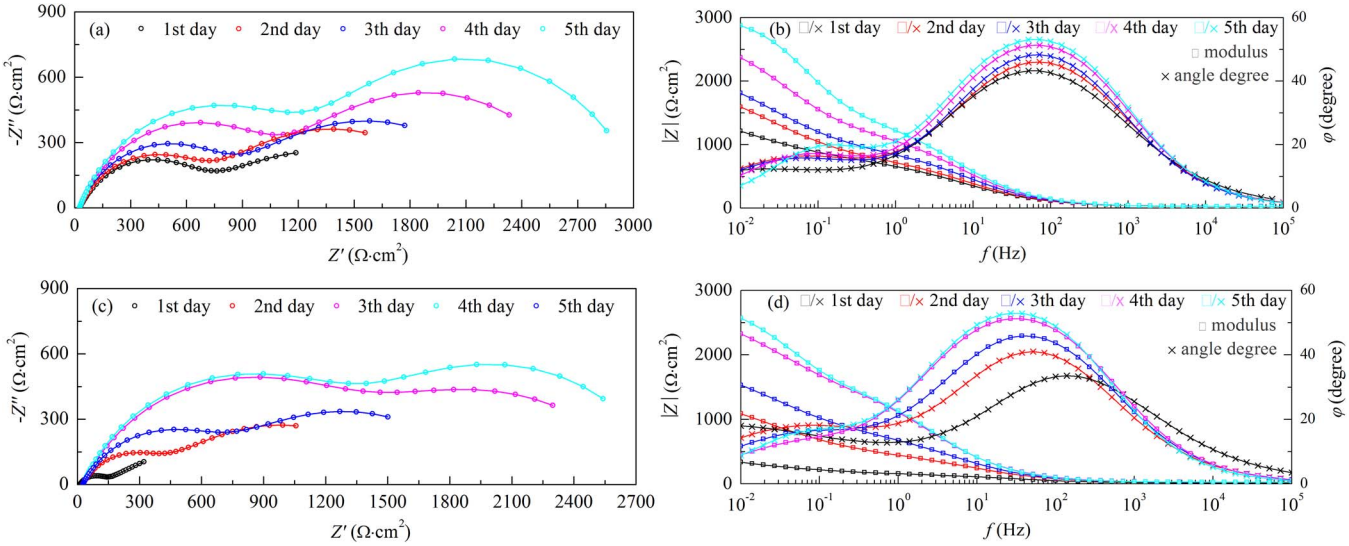


**Figure 7.** Nyquist impedance spectra for chalcopyrite (a) and chalcopyrite-pyrite (c), Bode plots and phase angles for chalcopyrite (b) and chalcopyrite-pyrite (d) in 9K solutions after different corrosion times, where ○, □ and × represent the experimental values, and – represents the simulated values.

**Table V. Equivalent circuit model parameters for the chalcopyrite electrode in 9K solutions.**

| | | $CPE_f$ | | | | $CPE_t$ | | | |
|---|---|---|---|---|---|---|---|---|---|
| Electrode | Soak time (day) | $Y_0$ ($S \cdot cm^{-2} \cdot s^{-n}$) | $n$ | $C_f$ ($F \cdot cm^{-2}$) | $R_f$ ($\Omega \cdot cm^2$) | $Y_0$ ($S \cdot cm^{-2} \cdot s^{-n}$) | $n$ | $C_t$ ($F \cdot cm^{-2}$) | $R_t$ ($\Omega \cdot cm^2$) |
| Galvanic corrosion chalcopyrite | 1 | 3.424E-4 | 0.655 | 6.146E-5 | 112.0 | 1.058E-2 | 0.375 | 7.138E-1 | 1183 |
| | 2 | 1.906E-4 | 0.701 | 6.100E-5 | 362.9 | 3.018E-3 | 0.533 | 9.381E-3 | 1209 |
| | 3 | 1.558E-4 | 0.706 | 6.000E-5 | 649.1 | 2.440E-3 | 0.579 | 5.689E-3 | 1313 |
| | 4 | 1.201E-4 | 0.720 | 5.842E-5 | 1305 | 2.130E-3 | 0.621 | 4.207E-3 | 1432 |
| | 5 | 1.085E-4 | 0.736 | 5.447E-5 | 1350 | 2.066E-3 | 0.734 | 3.111E-3 | 1497 |
| Self-corrosion chalcopyrite | 1 | 1.377E-4 | 0.687 | 4.502E-5 | 624.3 | 3.715E-3 | 0.450 | 2.778E-2 | 1396 |
| | 2 | 1.084E-4 | 0.705 | 3.611E-5 | 666.8 | 2.460E-3 | 0.583 | 6.052E-3 | 1431 |
| | 3 | 8.565E-5 | 0.728 | 3.127E-5 | 787.1 | 2.237E-3 | 0.587 | 5.399E-3 | 1564 |
| | 4 | 7.416E-5 | 0.731 | 2.919E-5 | 1070 | 1.860E-3 | 0.691 | 3.094E-3 | 1678 |
| | 5 | 6.621E-5 | 0.739 | 2.752E-5 | 1257 | 1.238E-3 | 0.791 | 1.526E-3 | 1784 |

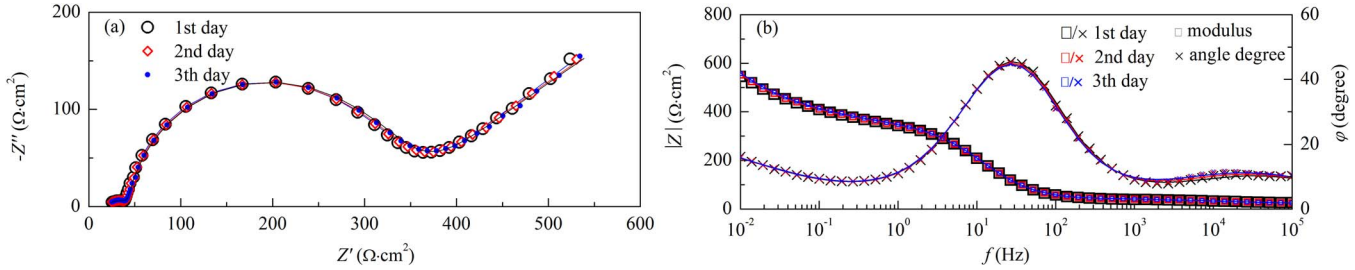


**Figure 9.** Nyquist impedance spectra (a), Bode plots and phase angles for the galvanic protect pyrite (b) for the galvanic protect pyrite in 9K solutions after the different corrosion times, where ○, □ and × represent the experimental values, and – represents the simulated values. Three Bode curves are shown since the repetition overlapped completely.

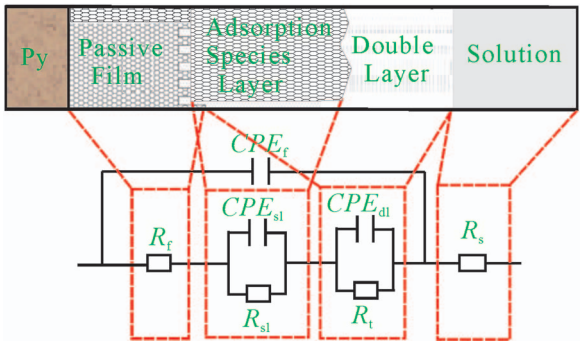


**Figure 10.** Equivalent circuit for the pyrite electrode in 9K solutions.

curves almost overlapped exactly, showing that the pyrite electrode was subjected to galvanic protection.

***Surface characterization measurements.***—Figure 11 shows the Raman spectra of chalcopyrite and pyrite samples under the galvanic corrosion condition. When pyrite connected with chalcopyrite, two Raman peaks at 342 and 378 $cm^{-1}$ were observed; they were two of the five theoretical Raman-active modes of pyrite[29–31] suggesting that the pyrite was in galvanic protection when connected with the chalcopyrite. When the pyrite sample was dipped in 9K solution alone, the Raman spectra showed a new peak at 432 $cm^{-1}$, except the two

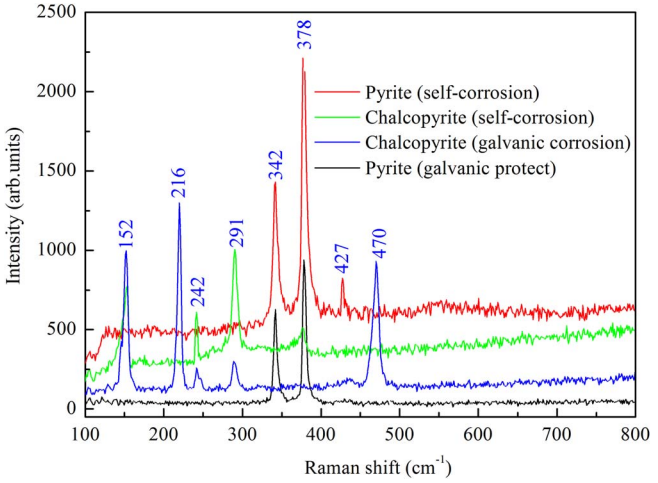


**Figure 11.** Raman spectra of the pyrite, and the chalcopyrite samples after galvanic corrosion or protection in 9K solution.

pyrite characteristic peaks 342 and 378 $cm^{-1}$. Li et al.[32] reported that the Raman peak at 432 $cm^{-1}$ was assigned to the vibration mode of the S-S bond of elemental sulfur, suggesting that the pyrite was eroded and produced S. For chalcopyrite, when it was dipped in 9K

**Table VI. Equivalent circuit model parameters for the pyrite electrode in 9K solutions.**

| $CPE_{dl}$ | | | | $CPE_{sl}$ | | | | $CPE_f$ | | | |
|---|---|---|---|---|---|---|---|---|---|---|---|
| $Y_{0,1}$ ($S \cdot cm^{-2} \cdot s^{-n}$) | $n_1$ | $C_t$ ($F \cdot cm^{-2}$) | $R_t$ ($\Omega \cdot cm^2$) | $Y_{0,2}$ ($S \cdot cm^{-2} \cdot s^{-n}$) | $n_2$ | $C_{sl}$ ($F \cdot cm^{-2}$) | $R_{sl}$ ($\Omega \cdot cm^2$) | $Y_{0,3}$ ($S \cdot cm^{-2} \cdot s^{-n}$) | $n_3$ | $C_f$ ($F \cdot cm^{-2}$) | $R_f$ ($\Omega \cdot cm^2$) |
| 1.008E-4 | 0.5204 | 7.251E-6 | 573.1 | 1.347E-2 | 0.438 | 3.138E-3 | 23.85 | 6.420E-5 | 0.954 | 5.308E-5 | 301.1 |

solution alone, the Raman spectra showed 3 Raman peaks at 152 $cm^{-1}$, 242 $cm^{-1}$ and 291 $cm^{-1}$. The Raman peaks at 152 $cm^{-1}$ and 242 $cm^{-1}$ were assigned to the vibration mode of the S-S bond of elemental sulfur.[32] The Raman peak at 291 $cm^{-1}$ was characteristic of a structure for chalcopyrite,[33] meaning that chalcopyrite was eroded and produced S. When chalcopyrite connected with pyrite and dipped in 9K solution alone, the Raman spectra showed another two Raman peaks at 216 $cm^{-1}$ 242 $cm^{-1}$ and 470 $cm^{-1}$; Li et al.[32] confirmed that these two peaks were also assigned to the vibration mode of the S-S bond of elemental sulfur.

## Conclusions

The present study addressed the pyrite-assisted leaching of chalcopyrite and presented the in situ electrochemical parameters. The experiments showed that the presence of pyrite is advantageous to chalcopyrite leaching, and the leaching efficiency increases with increasing pyrite or Py/Cp ratio. In the absence of the addition of pyrite (Py/Cp = 0), chalcopyrite was leached at an approximate rate of 0.03 g/L/day. This rate increased to approximately 0.29 g/L/day when Py/Cp = 5, and the ratio of pyrite to chalcopyrite in the leached residue increased from 1.7 to 12 when Py/Cp was increased from 1 to 3. The OCP experiments showed that pyrite and chalcopyrite electrodes were approximately 421.32 ± 5 mV and 320.63 ± 5 mV, respectively, suggesting that pyrite acts as a cathode and the chalcopyrite acts as an anode when in the same electrolyte system. Polarization curves show that the $i_{couple}/i_{corr}$ value was 1.71 at a cathode to anode area ratio ($S_c/S_a$) of 1:1. Galvanic corrosion tests of current confirmed that the chalcopyrite leaching selectivity improved with increasing Py/Cp ratio. Finally, the EIS results showed that the chalcopyrite electrochemical dissolution (leaching) rate depended on the charge transfer at the double layer and passive film characters, and the chalcopyrite corrosion rate decreased as soak time continued. The presence of pyrite promoted the chalcopyrite electrochemical dissolution and subjected itself to galvanic protection.

## Acknowledgments

This work was financially supported by the National Key R&D Program of China (grant No. 2016YFC0600104), Large-scale Scientific Apparatus Development Program of the Chinese Academy of Sciences (grant No. YZ200720), and the "135" Program of the Institute of Geochemistry, Chinese Academy of Sciences (CAS).

## ORCID

Heping Li https://orcid.org/0000-0001-7814-0589

## References

1. X. M. Chen, Y. J. Peng, and D. Bradshaw, *Miner. Eng.*, **58**, 64 (2014).
2. Y. F. Mu, Y. J. Peng, and R. A. Lauten, *Miner. Eng.*, **122**, 91 (2018).
3. D. H. Kim, W. J. Kim, H. S. Kim, K. S. Han, T. Tran, and M. J. Kim, *J. Min. Metall. B.*, **52**, 119 (2016).
4. Y. Li, N. Kawashima, J. Li, A. P. Chandra, and A. R. Gerson, *Adv. Colloid Interfac.*, **197–198**, 1 (2013).
5. A. P. Mehta and L. E. Murr, *Biotechnol. Bioeng.*, **24**, 919 (1982).
6. A. P. Mehta and L. E. Murr, *Hydrometall.*, **9**, 235 (1983).
7. D. G. Dixon, D. D. Mayne, and K. G. Baxter, *Can. Metall. Q.*, **47**, 327 (2008).
8. O. G. Olvera, L. Quiroz, D. G. Dixon, and E. Asselin, *Electrochim. Acta*, **127**, 7 (2014).
9. Y. B. Li, G. J. Qian, P. L. Brown, and A. R. Gerson, *Geochim. et Cosmochim. Acta*, **212**, 33 (2017).
10. S. N. Tan and M. Chen, *Hydrometall.*, **119–120**, 87 (2012).
11. A. I. Vogel and G. H. Jeffery, *Vogel's textbook of quantitative chemical analysis*, Longman Scientific & Technical; Wiley, Harlow, Essex, England: New York, xxix, pp. **877**(1978).
12. Bruker, TOPAS, Version 4.2 Bruker AXS Inc., Madison, Wisconsin, USA (2009).
13. S. M. J. Koleini, V. Aghazadeh, and A. Sandstrom, *Miner. Eng.*, **24**, 381 (2011).
14. A. F. Tshilombo, *Mechanism and kinetics of chalcopyrite passivation and depassivation during ferric and microbial leaching*, University of British Columbia, Vancouver (2004).
15. N. Hiroyoshi, M. Hirota, T. Hirajima, and M. Tsunekawa, *Hydrometall.*, **47**, 37 (1997).
16. E. M. Córdoba, J. A. Muñoz, M. L. Blázquez, F. González, and A. Ballester, *Hydrometall.*, **93**, 88 (2008).
17. S. M. J. Koleini, M. Jafarian, M. Abdollahy, and V. Aghazadeh, *Ind. Eng. Chem. Res.* **49**, 5997 (2010).
18. E. T. Pecina, A. Uribe, J. A. Finch, and F. Nava, *Miner. Eng.*, **19**, 904 (2006).
19. P. R. Holmes and F. K. Crundwell, *Hydrometall.*, **39**, 353 (1995).
20. A. J. Bard and L. R. Faulkner, *Electrochemical methods: fundamentals and applications*, 2nd. Hoboken: Wiley and Sons (2001).
21. S. L. d. Assis, S. Wolynec, and I. Costa, *Electrochim. Acta*, **51**, 1815 (2006).
22. Z. F. Yin, M. L. Yan, Z. Q. Bai, W. Z. Zhao, and W. J. Zhou, *Electrochim. Acta*, **53**, 6285 (2008).
23. F. T. Cheng, K. H. Lo, and H. C. Man, *Surf. Coat. Tech.*, **172**, 316 (2003).
24. J. R. Macdonald, *J. Appl. Phys.*, **58**, 1971 (1985).
25. B. Hirschorn, M. E. Orazem, B. Tribollet, V. Vivier, I. Frateur, and M. Musiani, *Electrochim. Acta*, **55**, 6218 (2010).
26. Y. Sun, D. Lv, J. Zhou, X. Zhou, Z. Lou, S. A. Baig, and X. Xu, *Chemosphere*, **185**, 452 (2017).
27. C. Weisener and A. Gerson, *Surf. Interface Anal.*, **30**, 454 (2015).
28. P. Velásquez, D. Leinen, J. Pascual, J. R. Ramos-Barrado, P. Grez, H. Gómez, R. Schrebler, R. D. RÍo, and R. Córdova, *J. Phys. Chem. B*, **109**, 4977 (2005).
29. J. R. Mycroft, G. M. Bancroft, N. S. Mcintyre, J. W. Lorimer, and I. R. Hill, *J. Electroanal. Chem. Interf. Electrochem.*, **1**, 139 (1990).
30. S. B. Turcotte, R. E. Benner, A. M. Riley, J. Li, M. E. Wadsworth, and D. M. Bodily, *J. Electroanal. Chem.*, **1–2**, 195 (1993).
31. M. M. Mcguire, K. N. Jallad, D. Ben-Amotz, and R. J. Hamers, *Appl. Surf. Sci.*, **1**, 105 (2001).
32. J. Li, X. Zhu, and M. E. Wadsworth, Raman spectroscopy of natural and oxidized metal sulfides. In: J. P. Hager, (Ed.), EPD Congress, *the Minerals, Metals and Materials Society*. 229 (1993).
33. T. P. Mernagh and A. G. Trudu, *Chem. Geol.*, **103**, 113 (1993).